Contents lists available at ScienceDirect

Transactions of Nonferrous Metals Society of China

36(2026) 727−739

www.tnmsc.cn

Optimization of ZK60 magnesium alloy properties via secondary extrusion of rapidly solidified strips

Zhen-shuai LI [a,b], Chao YANG [a,b], Shuai BAO [a,b], Yun-gui CHEN [a,c,*]

[a] Institute of New Energy and Low-Carbon Technology, Sichuan University, Chengdu 610207, China;

[b] School of Materials Science and Engineering, Sichuan University, Chengdu 610065, China;

[c] Engineering Research Center of Alternative Energy Materials & Devices of Ministry of Education, Sichuan University, Chengdu 610065, China

Abstract: The microstructure and mechanical properties of ZK60 extruded alloy by rapid solidification (RS) and as-cast ingot processes were investigated using optical microscope, scanning electron microscope, X-ray diffraction, electron back-scatter diffraction, and mechanical tests. The results show that the RS ZK60 extruded alloy exhibits relatively high tensile yield strength (TYS), compressive yield strength (CYS) and elongation of 300.8 MPa, 303.6 MPa and 18.6%, respectively. The RS ZK60 extruded alloy with an ultra-fine grain size of 1.28 μm not only has a weak texture with a maximum polar density of 3.3 but also addresses the tension−compression asymmetry with a CYS/TYS ratio of approximately 1.0. The calculation of the strengthening mechanism indicates that the improvement in the mechanical properties of the RS ZK60 extruded alloy is primarily attributed to grain refinement.

Keywords: ZK60 magnesium alloy; rapid solidification; hot extrusion; tension−compression asymmetry; texture; strengthening mechanism

1 Introduction

In recent years, owing to concerns about energy conservation and environmental issues, efforts have been made to apply lightweight materials. Magnesium alloys, with their low density, high specific strength and stiffness, high recovery rate, and other advantageous properties, have gained widespread attention in lightweight applications, such as automobiles, aircraft, and electronic consumer products [1]. However, due to their low strength and poor plastic deformation ability, magnesium alloys face limitations in widespread application, with their yield being much lower than that of steel and aluminum alloys. As a result, improving the mechanical properties of magnesium alloys has become an important research topic [2,3].

There are several ways to improve the mechanical properties of alloys: for one thing, the addition of alloying elements, especially rare earth elements, and for another, innovative processing technology, such as rapid solidification (RS) and severe plastic deformation (SPD). Regarding the influence of rare earth elements, ZENGIN and TUREN [4] studied the effects of La content on the microstructure and mechanical properties of ZK60 alloy. The ZK60−1La alloy showed a superior yield strength of 311 MPa and elongation of 13%. In addition, LIU et al [5] obtained a high yield strength of 389 MPa by adding 1% Ce and 0.5% Y to ZK60 alloy, but the elongation was only 3.5%. DENG et al [6] improved the mechanical properties and thermal stability of magnesium alloys by adding

Corresponding author: *Yun-gui CHEN, Tel: +86-13981815102, E-mail: chenyungui@scu.edu.cn

https://doi.org/10.1016/S1003-6326(25)66993-7

Received 30 May 2024; accepted 2 March 2025

rare earth elements Gd and Sm, which formed thermally stable lath-like intermetallic particles. After extrusion and aging treatment of Mg−Gd−Zr rare earth magnesium alloys, YANG et al [7] showed that there were large densities of basal stacking faults and profuse distortion areas in the non-recrystallized grains, which improved the tensile and compression asymmetry and the yield strength of the alloys. In general, the addition of rare earth elements can optimize the microstructure of magnesium alloys, such as grains, texture, phase morphology and distribution, thus improving the mechanical properties. However, the associated costs need to be taken into account.

Grain refinement, as described by the Hall−Petch equation, is an effective method to enhance the strength of metal materials, particularly magnesium alloys, due to their high strengthening factor [8,9]. Grain refinement can be achieved by RS and SPD. RS is typically achieved through single-roll melt-spinning or alloy melt atomization, producing powders, flakes, or strips, which require further metallurgical consolidation, such as hot extrusion, to form bulk material [10]. Compared to conventional magnesium alloys, rapid solidification/powder metallurgy (RS/PM) magnesium alloys exhibit remarkable strength and ductility. ZHOU et al [11] obtained a tensile yield strength of 353 MPa at room temperature and a strength of 202 MPa at 200 °C for Mg−6Zn−5Ca alloy by RS/PM, which was mainly attributed to grain refinement and the distribution of fine dispersed phases. KULA et al [12] compared the microstructure and properties of RS and as-cast AM60 alloys, and obtained that RS alloy exhibited better mechanical properties due to fine grains and highly dispersed nanoscale intermetallic particles. NISHIMOTO et al [13] obtained a high strength and toughness Mg−Zn−Y−Al alloy with a yield strength greater than 400 MPa and elongation exceeding 10% by RS ribbon consolidation. Usually, RS/PM not only refine the grain directly but also optimizes the texture by subsequent plastic deformation.

For wrought magnesium alloys, direct SPD is an effective method to improve their mechanical properties. For instance, FAN et al [14] proposed a new method for repeated upsetting and extrusion deformation of AZ31 magnesium alloy, resulting in the refinement of dynamically recrystallized grains to 0.8 μm and a significant increase in hardness. ZHANG et al [15] proposed a novel closed-forging extrusion process for AZ31 magnesium alloy, which effectively refines the grain size and improves the strength, plasticity, and anisotropy of the alloy. YING et al [16] analyzed the influence of the extrusion process on the mechanical properties of ZK60 alloy and increased the yield strength and elongation to 328 MPa and 13.8% by extrusion and ECAP. YANG et al [17] investigated Mg−8Zn−6Al extruded alloys containing quasicrystal precipitates at an extrusion temperature of 240 °C and an extrusion speed of 0.1 mm/s, where pyramidal $\langle c+a \rangle$ and prismatic $\langle c \rangle$ dislocations and tensile twinning in the texture grains were activated under compression, leading to the reversed yield strength asymmetry. ZHANG et al [18] used an asymmetric lowered-temperature rolling technique to obtain fine-grained ZK60 magnesium alloy sheets with a weak basal texture, and the yield strength of the rolled sheets increased from 157 to 216 MPa. In general, SPD can refine the grain, optimize the texture, and improve the mechanical properties of the alloy. However, the complexity of the technology increases manufacturing costs and process control difficulties.

This work aims to address the issues of low yield strength, pronounced texture, and tension-compression asymmetry in magnesium alloys, while providing insights for industrial production based on high efficiency and low cost. Based on this, the microstructure and mechanical properties of ZK60 alloy prepared by single-roll melt-spinning combined with high-speed hot extrusion were studied and compared with those prepared by conventional casting.

2 Experimental

A commercial ZK60 magnesium alloy was purchased, and its chemical composition is listed in Table 1. ZK60 thin strips with a width of 2−3 mm and a thickness of 50−80 μm were prepared by melt-spinning. The RS strips were crushed by mechanical shearing into millimeter-sized particles. These particles were pressed at 300 MPa and 250 °C into a hot-pressed ingot with a diameter of 42 mm and a height of 50 mm, prior to extrusion. The hot-pressed ingot was first extruded at 400 °C at an extrusion ratio of 3∶1 into a rod with a diameter of 24 mm.

Table 1 Chemical composition of commercial ZK60 magnesium alloy (wt.%)

Zn	Zr	Mn	Si	Fe	Cu	Ni	Al	Mg
5.64	0.48	0.035	0.0017	0.0012	0.0021	0.0005	0.0012	Bal.

Subsequently, it was secondarily extruded at 350 °C with a ram speed of 5 mm/s, achieving a final diameter of 5 mm, which is referred to as the RS ZK60 extruded rod. For comparison, the purchased ZK60 magnesium alloy was re-melted and cast into an ingot with a diameter of 24 mm at 720 °C under a protective atmosphere of CO_2+SF_6. After solid solution treatment at 400 °C for 24 h, the cast ingot was extruded into a *d*5 mm rod using the same parameters as the RS ZK60 rod, referred to as the as-cast ZK60 extruded rod.

After polishing and etching with 4% nitrate solution, the microstructure of the as-cast and RS ZK60 ingot, as-cast and RS ZK60 extruded rod was observed by optical microscope (OM, MDS400) and field emission scanning electron microscope (FESEM, REGULUS 8230). X-ray diffraction (XRD) analysis was used to investigate the phases existing in different conditions using an X-ray diffractometer (Rigaku SmartLab) with Cu K_α radiation over a range of 5°−90° (0.013° step size). Test samples were alloy powders extracted from the specimens. Phase refinement and crystallographic analysis were performed using GSAS software. Electron backscatter diffraction (EBSD) was used to analyze the grain size, grain orientation, and texture parameters, such as the maximum strength, average Schmid factor, and average particle size, using AZtecCrystal software to process the results. EBSD was performed using a Symmetry S2 detector with a step size of 0.1 μm, a voltage of 20 kV, and an inclination angle of 70°. EBSD samples were selected from the central region along the extrusion direction using spark erosion wire cutting, and samples were first mechanically polished and then argon ion polished (voltage 6 kV, inclination angle 6°, and polishing time 30 min).

Extruded rods were machined into tensile test samples with a gauge diameter of 4 mm and a gauge length of 25 mm. In addition, compression test samples were also prepared with a diameter of 5 mm and a height of 6 mm. The tests were carried out on a universal testing machine (INSTRON 5967) at a strain rate of 2.5×10^{-4} s^{-1}.

3 Results and discussion

3.1 Microstructure and phases analysis

Figure 1(a) shows a typical microstructure of the as-cast ZK60 alloy. A nearly continuous $MgZn_2$ phase is distributed along the boundary. As shown in Fig. 1(b), after solid solution treatment, almost all of the $MgZn_2$ phases dissolved into the α-Mg matrix.

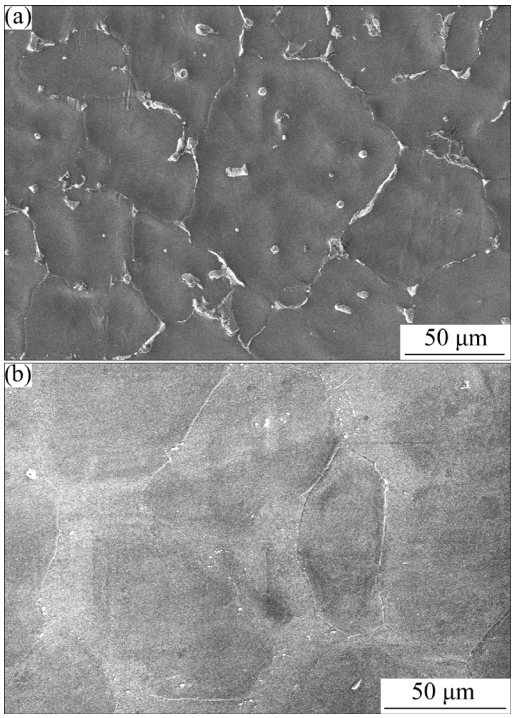

Fig. 1 SEM images of as-cast ZK60 ingot before (a) and after (b) solution treatment

Figure 2 shows optical microscope (OM) images of the RS ZK60 ingot. The particles at the circumference of the ingot were fine and uniform, with no visible interfaces between them. However, some isolated tiny pores remain, as indicated by red arrows in Fig. 2(a). In the central part, the particles consist of both large and small grains, with visible interfaces between them, as indicated by the blue dotted line in Fig. 2(b). Continuous tiny pores at the particle interfaces are indicated by red arrows. The friction force on the circumference of the extruded ingot results in great stress and deformation,

promoting dynamic recrystallization, fine grain formation, and improved metallurgical bonding.

The XRD patterns of ZK60 magnesium alloy under different conditions are shown in Fig. 3. There was only α-Mg phase in both the as-cast and RS ingots, and the diffraction peak of any secondary phase did not appear after hot extrusion deformation. However, the diffraction peak intensity, especially for the $(10\bar{1}0)$ and (0002) planes, changed in comparison with that of the standard diffraction peak for Mg. The RS ingot exhibited a high diffraction peak intensity, while the RS extruded rod showed a low intensity.

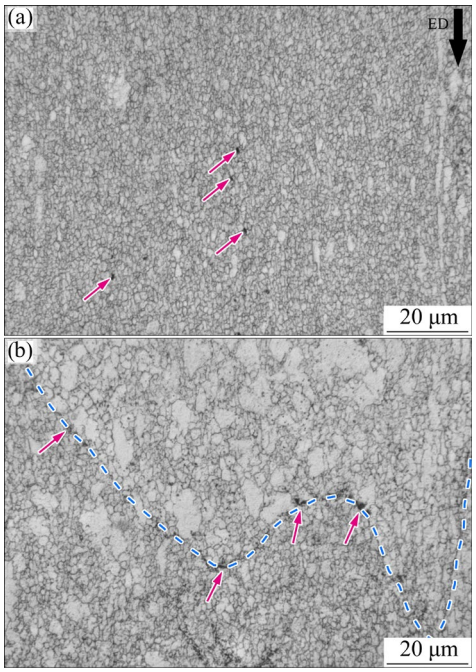

Fig. 2 OM images of RS ZK60 ingot: (a) Circumference; (b) Center

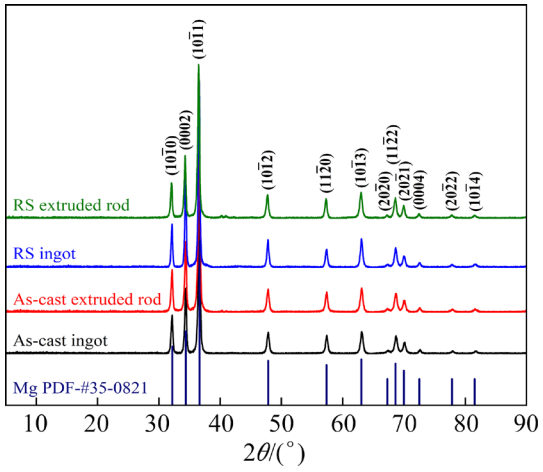

Fig. 3 XRD patterns of ZK60 alloy under different conditions

XRD Rietveld refinement of the ZK60 extruded rods in different states was performed to study the effect of rapid solidification on lattice parameters, as shown in Fig. 4 and Table 2. The a, c, and cell volume of the α-Mg phase in the RS ZK60 extruded rod were smaller than those in the as-cast extruded rod, and the c/a ratio showed no significant change (Table 2). This is due to the rapid solidification process, which increases the solid solubility of Zn atoms in the Mg matrix, thereby altering its lattice parameters.

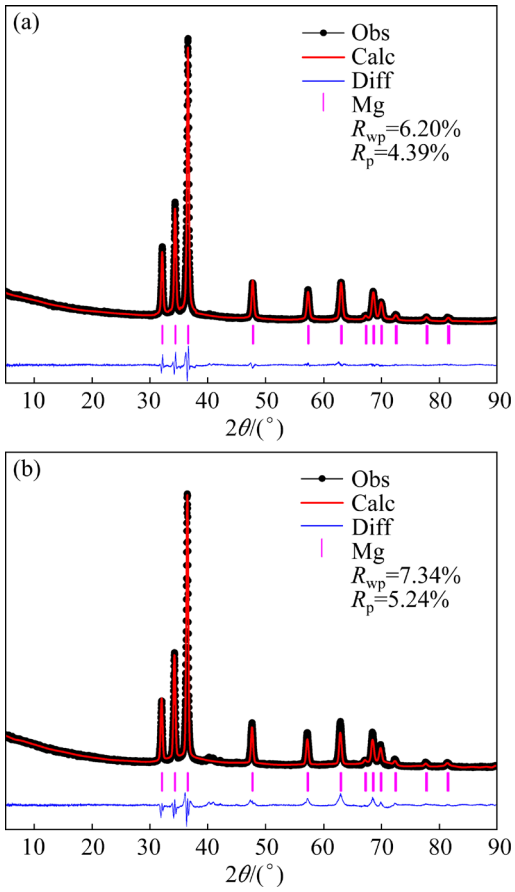

Fig. 4 Rietveld refinement XRD patterns of ZK60 extruded rods in different states: (a) As-cast; (b) RS

Table 2 Refined parameters of extruded rods

Sample	$a=b$/Å	c/Å	V/Å^3	c/a
ID: 4111965 [19]	3.2344	5.2527	47.588	1.624
As-cast	3.2111	5.2112	46.534	1.623
RS	3.2000	5.1943	46.063	1.623

3.2 Mechanical properties

The stress−strain curves of the RS and as-cast ZK60 extruded rods are shown in Fig. 5(a), with the relevant mechanical properties in Table 3. The

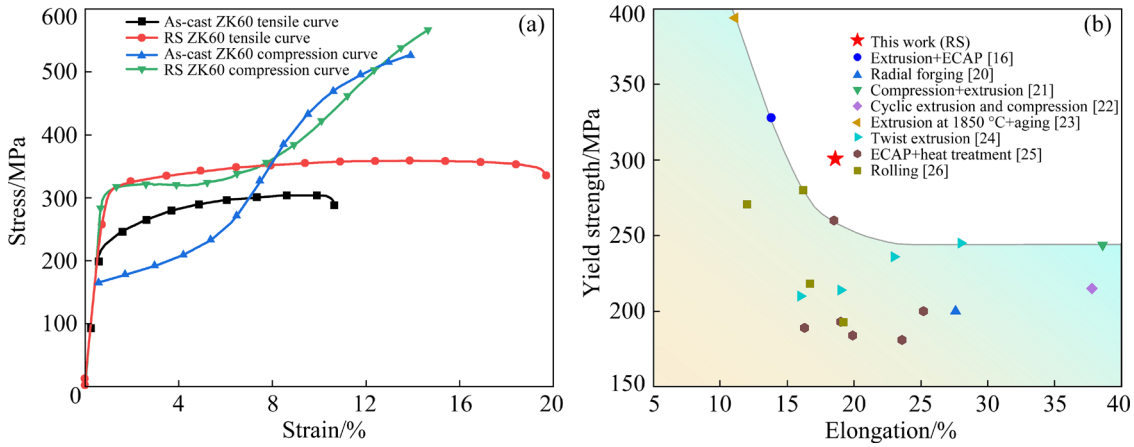

Fig. 5 (a) Mechanical properties of RS and as-cast ZK60 extruded rods; (b) Tensile properties of ZK60 alloys in comparison with available literature data

Table 3 Tensile and compression properties of extruded rods

Sample	Tensile property				Compression property				CYS/TYS
	TYS/MPa	UTS/MPa	EL/%	*E*/GPa	CYS/MPa	UCS/MPa	EL/%	*E*/GPa	
As-cast	220.9±2.4	304.8±8.4	9.7±1.3	42.4	160.2±7.2	524.9±1.6	12.8±2.3	44.6	0.725
RS	300.8±1.2	359.1±4.1	18.6±1.5	43.7	303.6±2.3	563.8±10.3	13.4±1.7	45.3	1.009

E: Elastic modulus

tensile yield strength (TYS), ultimate tensile strength (UTS), and elongation (EL) were 300.8 MPa, 359.1 MPa and 18.6% for the RS ZK60 extruded rod, and 220.9 MPa, 304.8 MPa and 9.7% for the as-cast ZK60 extrusion rod, respectively. The TYS, UTS, and EL of the RS ZK60 extruded rod increased by 36.2%, 17.8%, and 91.8%, respectively, compared to those of the as-cast ZK60 extrusion rod.

The compressive yield strength (CYS) increased from 160.2 MPa in the as-cast ZK60 extrusion rod to 303.6 MPa in the RS ZK60 extruded rod, where the raising rate of yield strength for the RS ZK60 magnesium alloy has a very significant value of 89.5%. At the same time, the CYS/TYS ratio increased significantly from 0.725 in the as-cast ZK60 extrusion rod to 1.009 in the RS ZK60 extruded rod, which expanded the range of industrial applications for magnesium alloys.

Figure 5(b) shows the mechanical properties of processed ZK60 magnesium alloys in this work and the published data on ZK60 magnesium alloys processed using different methods, i.e., extrusion + ECAP [16], radial forging [20], compression + extrusion [21], cyclic extrusion and compression [22], extrusion at 180 °C + aging [23], twist extrusion [24], ECAP + heat treatment [25] and rolling [26]. Compared to the above processes, the RS process is beneficial to improving the mechanical properties of ZK60 magnesium alloy.

3.3 Strengthening and toughening mechanisms

In general, the strength of a material increases at the cost of a decrease in plasticity. The strength and plasticity of the ZK60 alloy were improved by RS and hot extrusion.

3.3.1 Grain size distribution

EBSD was used to analyze the microstructure of the RS ZK60 and as-cast ZK60 extruded rods, as shown in Fig. 6. The observation direction of the extruded rod was along the extrusion direction (ED). After hot extrusion deformation, the grains of the RS ZK60 extruded rod were fine and uniform, and there was no obvious orientation along the ED, as shown in Fig. 6(a). However, the grains of the as-cast ZK60 extruded rod were unevenly distributed, consisting of long columnar grains and fine equiaxed grains, and the long columnar grains were distributed along the extrusion direction, as shown in Fig. 6(b). On the other hand, the area fraction of the low-angle grain boundaries (LAGBs) of the as-cast ZK60 extruded rod was 26.5% in Fig. 6(b), but that of the RS ZK60 extruded rod was only 7.85% in Fig. 6(a), where the

white line represents the LAGBs (<15°) and the black line represents the high-angle grain boundaries (HAGBs >15°).

The grain size statistic results are shown in Fig. 7. The grain size of the RS ZK60 extruded rod is 1.28 μm in Fig. 7(a). While that of the as-cast ZK60 extruded rods has a double peak distribution characteristics in Fig. 7(b), where the grain size at Peak 1 is less than 45 μm, and the average grain size is 11.29 μm, with an area fraction of 84.15%, while the grain size at Peak 2 is 111.89 μm, with an area fraction of 15.85%. Thus, the grain size of the as-cast ZK60 extruded rod is much larger than that of the RS ZK60 extruded rod.

Figures 6 and 7 indicate that the coarse microstructure of the as-cast ZK60 ingot can lead to inhomogeneous dynamic recrystallization and a double peak deformation microstructure, whereas the ultra-fine microstructure of the RS ZK60 ingot is likely to promote the occurrence of uniform dynamic recrystallization and a fine deformation microstructure.

During the hot extrusion process, dislocations were generated in the grains and gradually accumulated to form LAGBs, that is, subcrystal grains. When the orientation difference angle reaches the critical value θ_c (θ_c=15°) or dynamic recrystallization occurs, the number of HAGBs increases [27]. The grain boundary orientation differences between the RS and as-cast ZK60 extruded rods are shown in Fig. 8. The LAGBs of the RS ZK60 extruded rod were only 7.85%, as shown in Fig. 8(a), while those of the as-cast ZK60 extruded rod were 26.5%, as shown in Fig. 8(b). The former has fewer LAGBs, indicating that the ultrafine-grained RS ZK60 alloy undergoes greater dynamic recrystallization during hot extrusion, converting more LAGBs into HAGBs. However, the as-cast ZK60 alloy had coarse grains in the initial microstructure, and some coarse grains with hard orientation had difficulty undergoing dynamic recrystallization, resulting in more LAGBs and long coarse grains after hot extrusion, as shown in Fig. 6(b).

During the extrusion, the alloy forms HAGBs and LAGBs, and the grain boundary strengthening of

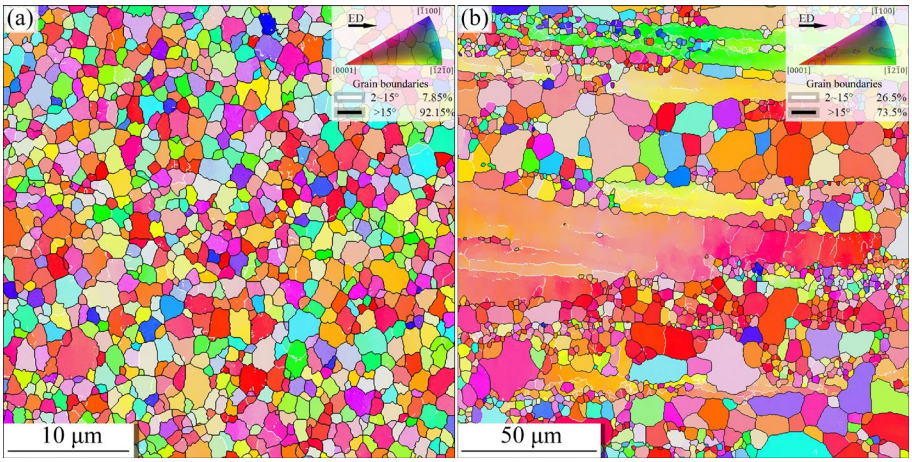

Fig. 6 EBSD maps of ZK60 extruded rods: (a) RS; (b) As-cast

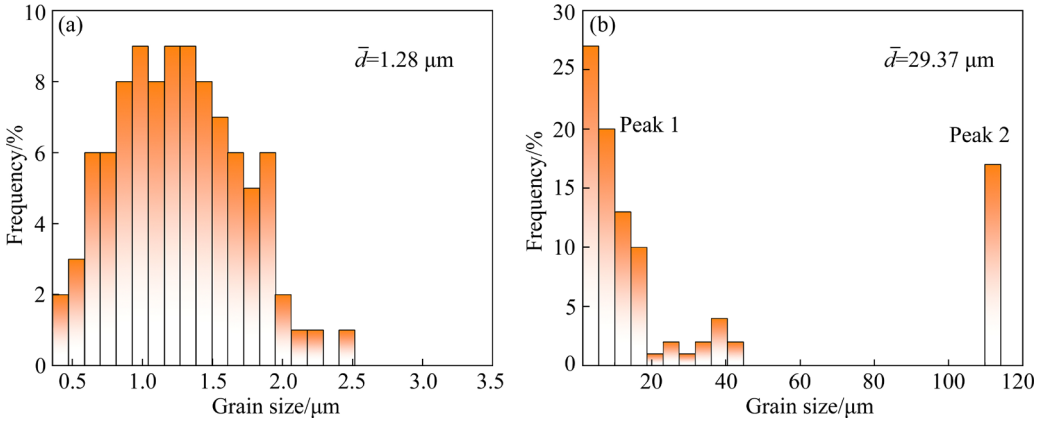

Fig. 7 Grain size distribution of ZK60 extruded rods: (a) RS; (b) As-cast

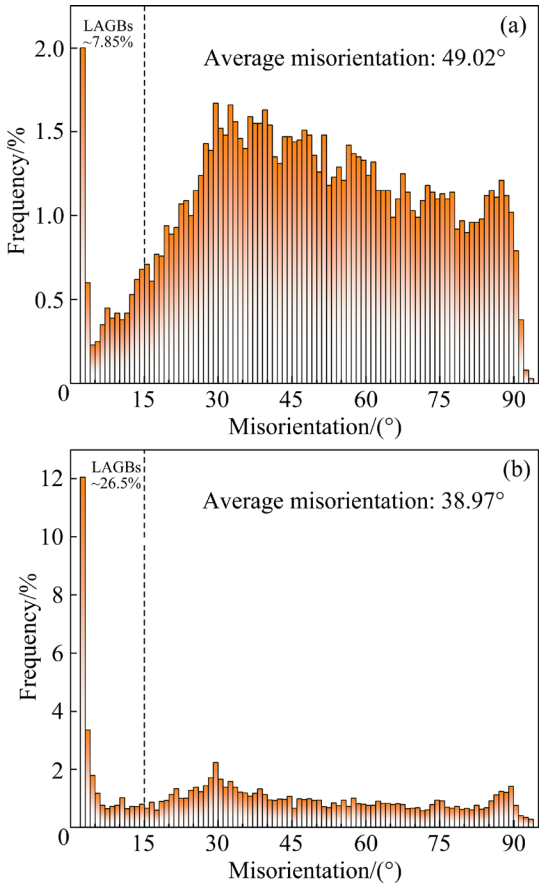

Fig. 8 Misorientation distribution of ZK60 extruded rods: (a) RS; (b) As-cast

the HAGBs can be described by the Hall−Petch formula [28,29]:

$$\sigma_{GB}=\sigma_0+kd^{-1/2} \quad (1)$$

where σ_{GB} is the yield stress of grain boundary strengthening, σ_0 (=145 MPa) is the friction stress for dislocation movement, k (=157 MPa·μm$^{-1/2}$) is the Hall−Petch coefficient [30], and d is the average grain size of the HAGBs. By calculating the grain sizes from Fig. 7, the tensile yield strength is 283.8 MPa for the RS ZK60 alloy and 186.7 MPa for the as-cast ZK60 alloy. The contribution of the grain size to yield strength in the RS ZK60 alloy is approximately 97.1 MPa higher than that in the as-cast ZK60 alloy. It can be observed that grain refinement can significantly improve the strength of the alloy.

3.3.2 Dislocation density and strengthening

The KAM value is the average orientation difference between a specific site and its neighbors and is related to the dislocation density of the material [31]. The KAM value can qualitatively reflect the uniformity of plastic deformation, with a higher value indicating greater plastic deformation or more defects. KAM diagrams of the RS and as-cast ZK60 extruded rods are shown in Fig. 9. The average KAM value of the RS ZK60 extruded rod was 0.36°, as shown in Fig. 9(a), whereas that of the as-cast ZK60 extruded rod was 0.6°, as shown in Fig. 9(b). At the same time, the larger KAM values of the as-cast ZK60 extrusion rod were mainly distributed around the LAGBs, as shown in Fig. 9(b), indicating uneven deformation.

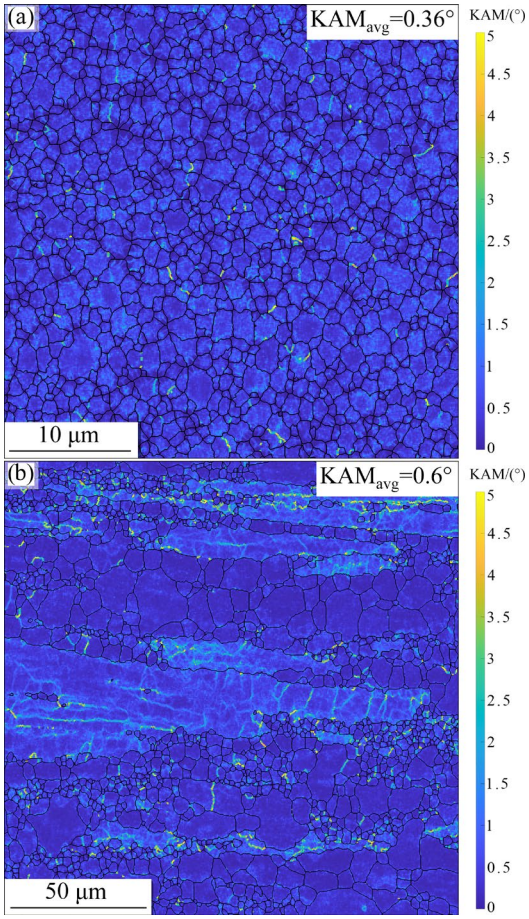

Fig. 9 KAM diagrams of ZK60 extruded rods: (a) RS; (b) As-cast

In the process of hot extrusion, an increase in dislocation density enhances the strength. In addition to the strengthening effect of HAGBs, LAGBs also play an important role in improving mechanical properties. The LAGBs can easily absorb the dislocations and induce dislocation strengthening. The LAGBs enhancement can be described by Formula (2) [27]:

$$\sigma_{LAGBs}=M\alpha Gb\rho_{LAGBs}^{1/2} \quad (2)$$

where M (=2.2) is the average Taylor factor, α (=0.2)

is a constant, G (=17 GPa) is the shear modulus, b (=0.32 nm) is the magnitude of Burgers vector, and ρ_{LAGBs} is the dislocation density of the LAGBs, which can be obtained from the KAM diagram. The dislocation density is not only related to the KAM value but also to the test step size [32]. The RS ZK60 was tested in steps of 0.1 μm, while the as-cast ZK60 was tested in steps of 0.4 μm due to grain inhomogeneity. Based on the EBSD model, ρ_{LAGBs}=7.1×10^{13} and 2.9×10^{13} m^{-2} were obtained for the RS and as-cast ZK60 alloy, respectively. From Formula (2), it can be calculated that σ_{LAGBs}= 20.2 MPa for the RS ZK60 alloy and 12.9 MPa for the as-cast ZK60 alloy, respectively. Therefore, the contribution of dislocation strengthening is limited.

3.3.3 Effect of texture

The pole figures of the RS and as-cast ZK60 extruded rods are shown in Fig. 10. The maximum texture intensities of the RS ZK60 extruded rod shown in Fig. 10(a) are 2.7, 3.3, and 2.3 in the (0001), $(10\bar{1}0)$, and $(2\bar{1}\bar{1}0)$ planes, respectively. However, the maximum texture intensities of the as-cast ZK60 extruded rod shown in Fig. 10(b) reach 7.6, 6.2, and 4.0 in the (0001), $(10\bar{1}0)$, and $(2\bar{1}\bar{1}0)$ planes, respectively. These facts indicate that the fine-grained structure reduces texture intensity, with little effect on the anisotropy of mechanical properties. Texture weakening is beneficial to improving tensile and compression asymmetry and strength [33].

In addition, the formation of the texture can affect the strength of the alloy. The contribution of texture strengthening (σ_t) can be described by Formula (3) [34]:

$$\sigma_t = m\tau_0 \tag{3}$$

where m is the orientation factor related to the basal texture, and τ_0 is the critical resolved shear stress (CRSS) for the slip system. According to previous research [35], the m is approximately 6.5 times the texture intensity of Mg alloys. The texture intensities of the basal plane for RS ZK60 and as-cast ZK60 alloys are 2.7 and 7.6, respectively, as shown in Fig. 10. Based on Ref. [36], the CRSS for basal slip $\{0001\}\langle 11\bar{2}0\rangle$ in a Mg signal crystal at room temperature is approximately 0.5 MPa. According to the calculations, σ_t is 8.8 MPa for the RS ZK60 alloy and 24.7 MPa for the as-cast ZK60 alloy.

Based on the above analysis, the mechanical properties of the ZK60 extruded magnesium alloy are mainly affected by grain boundary strengthening, dislocation strengthening, and texture strengthening. Figure 11 shows the tensile yield strength statistics of the extruded rods. Figure 11(a) shows the contributions of the different strengthening mechanisms, indicating that fine-grained strengthening

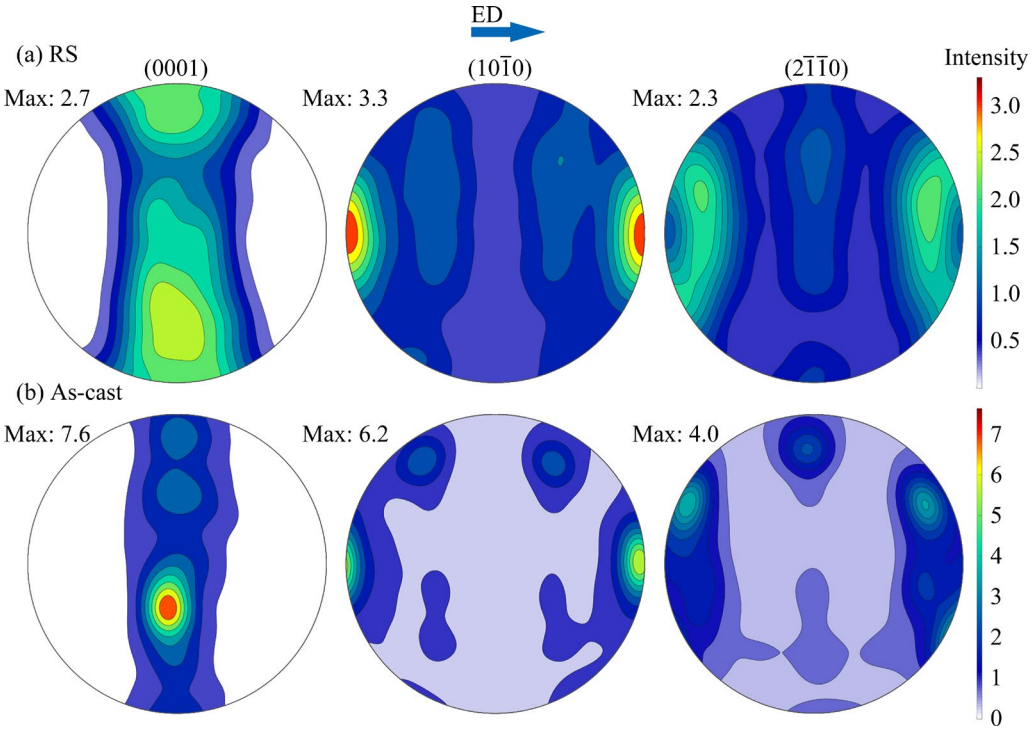

Fig. 10 Pole figures of ZK60 extruded rods: (a) RS; (b) As-cast

is dominant. Figure 11(b) compares the calculated and measured TYS values, with the calculated values closely matching the measured ones, confirming that the above strengthening mechanisms align with the actual results.

The plasticity of the RS ZK60 extruded magnesium alloy mainly depends on the grain size and texture intensity. The dynamic recrystallization behavior during hot extrusion results in ultrafine grains, which contributes to improved plasticity. The fine-grained structure reduces stress concentration and weakens the basal texture, facilitating basal plane slip [22, 37]. As shown in Fig. 10, the texture intensity of the RS ZK60 extruded rod is lower than that of the as-cast ZK60, and the RS ZK60 exhibits better plasticity.

3.3.4 Improvement of tension−compression asymmetry

OM images of the tensile and compression samples of the RS and as-cast ZK60 extruded rods are shown in Fig. 12. As shown in Fig. 12(a) for the tensile sample and Fig. 12(c) for the compressed sample, twins are hardly detected in the RS ZK60 extrusion rod, where the grains are fine and uniform, and deformation occurs mainly through

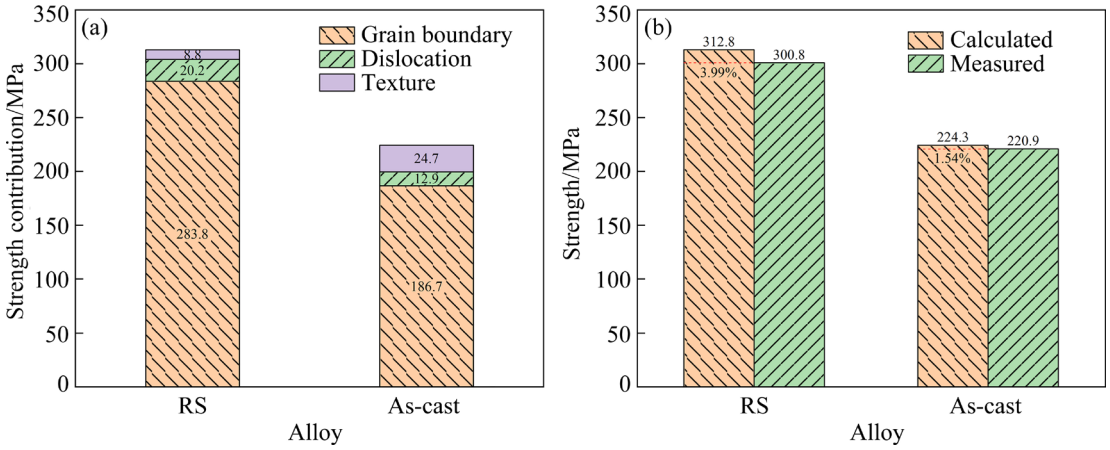

Fig. 11 Tensile yield strength statistics of ZK60 extruded rods: (a) Strength contribution calculated; (b) Comparison of calculated and measured values

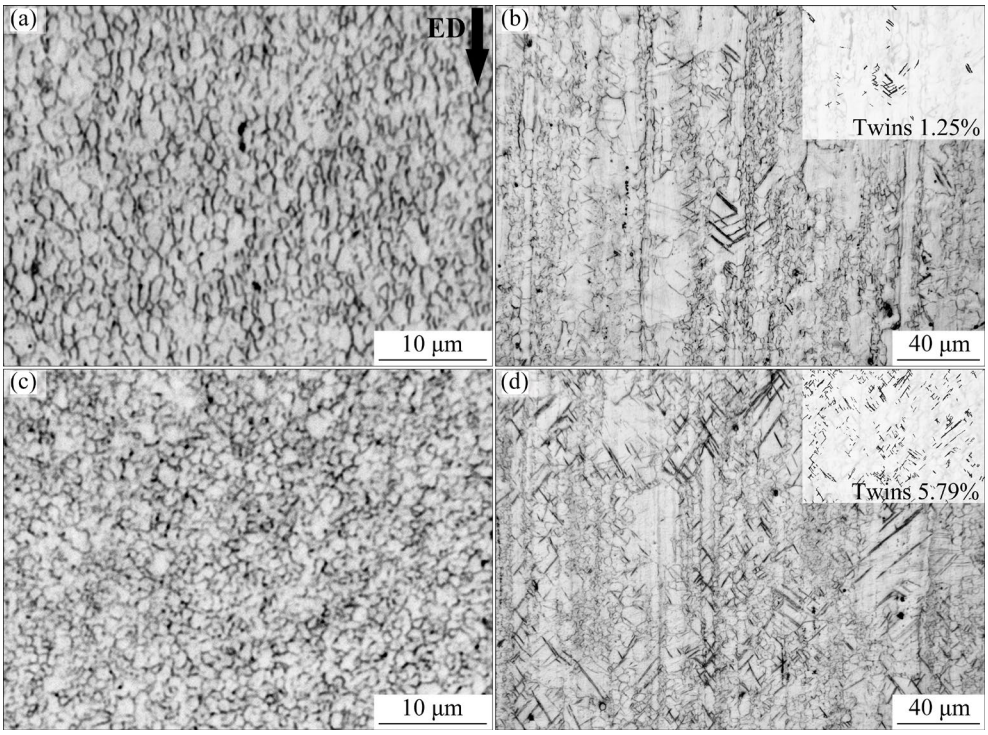

Fig. 12 OM images of ZK60 extruded rods: (a, b) RS and as-cast tensile samples, respectively; (c, d) RS and as-cast compressed samples, respectively

the coordination between grains. In contrast, the grains of the as-cast ZK60 extruded rod are coarse and unevenly distributed after tensile and compression, as shown in Figs. 12(b) and (d), with numerous twins forming within the coarse long-columnar grains. After statistical analysis, only 1.25% of the twins in the tensile sample is shown in Fig. 12(b), and 5.79% of the twins in the compression sample is shown in Fig. 12(d). This result indicates that it is easier to induce the formation of twins in the as-cast ZK60 extrusion rod with coarse grains, especially during the compression test, which leads to the tension−compression asymmetry of the alloy.

To explain the formation of twins, which leads to the tension−compression asymmetry in the as-cast ZK60 extrusion rod, the Schmid factor (SF) is further discussed in comparison with the RS ZK60 extrusion rod. SF is a well-established method for evaluating the grain orientation of magnesium alloy, which can evaluate the activation of slip systems. The higher the SF, the more slip systems can be activated [38]. The SFs of the basal, prismatic, pyramidal, and tensile twin slips are presented in Figs. 13 (a1−a4) for the RS ZK60 extruded rod and Figs. 13(b1−b4) for the as-cast ZK60 extruded rod.

Figures 13(a1) and (b1) show that the SFs of the RS and as-cast ZK60 extrusion rods at basal $\langle a\rangle$ are 0.22 and 0.15, respectively. Figure 13(b1) reveals that most of the basal planes have obvious hard orientations with SF of less than approximately 0.1 for the as-cast ZK60 extrusion rod, which corresponds well to the regions of coarse grains where twins occur, as shown in Figs. 12(b) and (d).

The critical resolved shear stress (CRSS) of pure Mg is 25 MPa for the slip system of $\{10\bar{1}0\}\langle 11\bar{2}0\rangle$ in the prismatic plane $\langle a\rangle$ and 200 MPa for that of $\{11\bar{2}2\}\langle 11\bar{2}3\rangle$ in the pyramidal plane $\langle a+c\rangle$ [39,40]. The SF is 0.42−0.45 for the prismatic $\langle a\rangle$ and pyramidal $\langle a+c\rangle$ in Figs. 13(a2) and (a3), (b2) and (b3) for both of the RS and as-cast ZK60 extrusion rods, all of which belong to the soft orientation during deformation. However, compared to the basal slip of only 0.5 MPa for the CRSS, the slip of these non-basal planes is hardly activated.

The SF of the $\{10\bar{1}2\}$ twin plane is high, 0.41 in Fig. 13(a4) for the RS ZK60 extrusion rod, and 0.43 in Fig. 13(b4) for the as-cast ZK60 extrusion rod. It is particularly evident in Fig. 13(b4) for the as-cast ZK60 extrusion rod, some Schmid factors approach 0.5. The CRSS is only 3.5 MPa for the $\{10\bar{1}2\}\langle 10\bar{1}1\rangle$ tensile twins [39], which is the main reason why magnesium alloys are prone to twinning at room temperature.

The reasons for the formation of twins in the as-cast ZK60 extrusion rod with coarse grains were analyzed in this study. Regarding the tension−compression asymmetry, BARNETT et al [41] showed that yield asymmetry is sensitive to texture in polycrystalline magnesium alloys. The texture intensity (7.6) of the as-cast ZK60 extrusion rod is about 2.8 times that (2.7) of the RS ZK60 extrusion rod, suggesting that the larger texture of the as-cast ZK60 extrusion rod is one of the main reasons for the tension−compression asymmetry.

In addition to the texture intensity affecting the tensile−compression asymmetry of magnesium alloys, grain size is an important influencing factor.

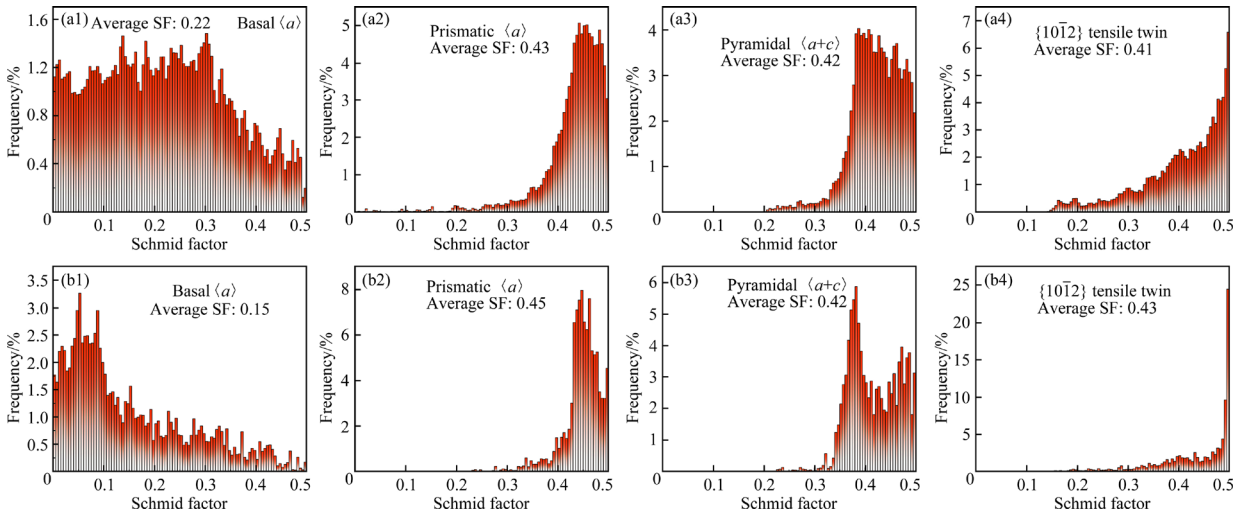

Fig. 13 Schmid factor diagrams of ZK60 extruded rods: (a1−a4) RS; (b1−b4) As-cast

The grains are fine enough that the stress required to activate twinning is greater than the slip [42]. In this case, slip dominates the deformation in both tensile and compressive processes, and the tensile−compressive asymmetry ceases to exist. According to the relevant literature [43], the yield asymmetry is almost non-existent when the AZ31 magnesium alloy grain is refined to 3.4 μm by multi-pass extrusion. It also evaluates a critical grain size of 0.8 μm without the appearance of yield asymmetry, regardless of whether the texture exists or not. Similar observations that the grain refinement eliminates yield asymmetry were also made by MISHRA et al [44] on friction stir processed (FSPed) Mg−Ag−RE alloys due to the ultra-fine grains generated by the process. In this work, the RS ZK60 extruded rod had an average grain size of only 1.28 μm, sufficiently fine to eliminate twinning and tension− compression asymmetry. The coarse grains in the as-cast ZK60 extrusion rod caused twin formation, especially in the compression process, leading to significant tension−compression asymmetry. Therefore, obtaining ultrafine grains by RS is an effective means of solving the tension−compression asymmetry for ZK60 and other magnesium alloys.

4 Conclusions

(1) The TYS, UTS, and EL of the RS ZK60 extruded alloy are 300.8 MPa, 359.1 MPa, and 18.6%, respectively, which are increased by 36.2%, 17.8%, and 91.8%, respectively, compared with those of the as-cast ZK60 extruded alloy. Meanwhile, the ratio of CYS/TYS increases from 0.725 to 1.009, indicating that rapid solidification can solve the problem of the tension−compression asymmetry of ZK60 deformed magnesium alloy.

(2) The grain of the RS ZK60 extruded rod is very fine and uniform with an average grain size of only 1.28 μm, while the as-cast ZK60 extruded rod exhibits a typical bimodal grain size distribution with one grain size of average 11 μm and another grain size of average 112 μm.

(3) The ultrafine grains caused by rapid solidification can significantly reduce the texture tendency of ZK60 deformed magnesium alloys. The polar densities of the RS ZK60 extruded rod in the (0001), $(10\bar{1}0)$, and $(2\bar{1}\bar{1}0)$ planes are only 2.7, 3.3, and 2.3, respectively, while those of the as-cast ZK60 extruded rod are 7.6, 6.2, and 4.0, respectively.

(4) The improvement in the strength of the RS ZK60 extruded magnesium alloy is mainly achieved by grain boundary strengthening, dislocation strengthening, and texture strengthening, where grain boundary strengthening is dominant. The yield strength of the RS ZK60 alloy is approximately 97 MPa higher than that of the as-cast ZK60 alloy, primarily due to the finer grain size.

CRediT authorship contribution statement

Zhen-shuai LI: Data curation, Investigation, Software, Writing – Original draft, Review & editing; **Chao YANG:** Project administration, Software, Supervision; **Shuai BAO:** Formal analysis, Resources, Validation; **Yun-gui CHEN:** Methodology, Conceptualization.

Declaration of competing interest

The authors declare that they have no known competing financial interests or personal relationships that could have appeared to influence the work reported in this paper.

Acknowledgments

This project is supported by Sichuan LTWT Metal Materials Co., Ltd., Sichuan Province, China (No. 21H1367).

References

[1] ZHANG Jian-yue, MIAO Jia-shi, BALASUBRAMANI N, CHO D H, AVEY T, CHANG Chia-yu, LUO A A. Magnesium research and applications: Past, present and future [J]. Journal of Magnesium and Alloys, 2023, 11: 3867−3895.

[2] LI Yuan-qi, LI Feng, KANG Fu-wei, DU Hua-qiu, CHEN Zi-yu. Recent research and advances in extrusion forming of magnesium alloys: A review [J]. Journal of Alloys and Compounds, 2023, 953: 170080.

[3] JIANG Bin, DONG Zhi-hua, ZHANG Ang, SONG Jiang-feng, PAN Fu-sheng. Recent advances in micro-alloyed wrought magnesium alloys: Theory and design [J]. Transactions of Nonferrous Metals Society of China, 2022, 32(6): 1741−1780.

[4] ZENGIN H, TUREN Y. Effect of La content and extrusion temperature on microstructure, texture and mechanical properties of Mg−Zn−Zr magnesium alloy [J]. Materials Chemistry and Physics, 2018, 214: 421−430.

[5] LIU Li-zi, CHEN Xian-hua, PAN Fu-sheng, GAO Shang-yu, ZHAO Chao-yue. A new high-strength Mg−Zn−Ce−Y−Zr magnesium alloy [J]. Journal of Alloys and Compounds, 2016, 688: 537−541.

[6] DENG Bo, LV Shu-hui, YANG Qiang, ZHAO Dong-yue, FAN Jun-yuan, QIU Xin. Lath-like phases formed at an extremely high temperature in a Mg−RE (RE = rare earth)−Al alloy [J]. Rare Metals, 2024, 43(8): 3937−3945.

[7] YANG Qiang, LV Shu-hui, GUAN Kai, XIE Ze-feng, QIU Xin. Extra-conventional strengthening mechanisms in non-

recrystallized grains of an extruded Mg−Gd−Zr alloy [J]. Journal of Magnesium and Alloys, 2024, 12(11): 4561−4573.

[8] LAKSHMANAN A, ANDANI M T, YAGHOOBI M, ALLISON J, MISRA A, SUNDARARAGHAVAN V. A combined experimental and crystal plasticity study of grain size effects in magnesium alloys [J]. Journal of Magnesium and Alloys, 2023, 11(12): 4445−4467.

[9] ZHENG Rui-xiao, GONG Wu, DU Jun-ping, GAO Si, LIU Mao-wen, LI Guo-dong, KAWASAKI T, HARJO S, MA Chao-li, OGATA S, TSUJI N. Rediscovery of Hall−Petch strengthening in bulk ultrafine grained pure Mg at cryogenic temperature: A combined in-situ neutron diffraction and electron microscopy study [J]. Acta Materialia, 2022, 238: 118243.

[10] AYMAN E, JUNKO U, KATSUYOSHI K. Application of rapid solidification powder metallurgy to the fabrication of high-strength, high-ductility Mg−Al−Zn−Ca−La alloy through hot extrusion [J]. Acta Materialia, 2011, 59(1): 273−282.

[11] ZHOU Tao, YANG Ming-bo, ZHOU Zhi-ming, HU Jian-jun, CHEN Zhen-hua. Microstructure and mechanical properties of rapidly solidified/powder metallurgy Mg−6Zn and Mg−6Zn−5Ca at room and elevated temperatures [J]. Journal of Alloys and Compounds, 2013, 560: 161−166.

[12] KULA A, TOKARSKI T, NIEWCZAS M. Comparative studies on the structure and properties of rapidly solidified and conventionally cast AM60 magnesium alloys [J]. Materials Science and Engineering: A, 2019, 759: 346−356.

[13] NISHIMOTO S, YAMASAKI M, KAWAMURA Y. Inherited multimodal microstructure evolution of high-fracture-toughness Mg−Zn−Y−Al alloys during extrusion for the consolidation of rapidly solidified ribbons [J]. Journal of Magnesium and Alloys, 2022, 10(9): 2433−2445.

[14] FAN Yu-tian, LU Li-wei, LIU Jian-bo, MA Min, HUANG Wei-ying, WU Rui-zhi. Effect of deformation temperature on microstructure and texture of AZ31 magnesium alloy processed by new plastic deformation method [J]. Transactions of Nonferrous Metals Society of China, 2024, 34(7): 2138−2152.

[15] ZHANG Kun-ming, QIN Chen, SHE Jia, JING Xue-rui, PENG Peng, TANG Ai-tao, RASHAD M, PAN Fu-sheng. Simultaneous improvement in strength and ductility of extruded Mg alloy via novel closed forging extrusion [J]. Transactions of Nonferrous Metals Society of China, 2022, 32(9): 2866−2876.

[16] YING Tao, HUANG Jian-ping, ZHENG Ming-yi, WU Kun. Influence of secondary extrusion on microstructures and mechanical properties of ZK60 Mg alloy processed by extrusion and ECAP [J]. Transactions of Nonferrous Metals Society of China, 2012, 22(8): 1896−1901.

[17] YANG Qiang, LV Shu-hui, YAN Zi-xiang, XIE Ze-feng, QIU Xin. Exceptional reversed yield strength asymmetry in a rare-earth free Mg alloy containing quasicrystal precipitates [J]. Journal of Magnesium and Alloys, 2024, 12(2): 687−699.

[18] ZHANG Wen-cong, LIU Xin-tong, MA Jun-fei, WANG Wen-ke, CHEN Wen-zhen, LIU Yu-xuan, YANG Jian-lei. Evolution of microstructure and mechanical properties of ZK60 magnesium alloy processed by asymmetric lowered-temperature rolling [J]. Transactions of Nonferrous Metals Society of China, 2022, 32(9): 2877−2888.

[19] SCHIMMEL H G, HUOT J, CHAPON L C, TICHELAAR F D, MULDER F M. Hydrogen cycling of niobium and vanadium catalyzed nanostructured magnesium [J]. Journal of the American Chemical Society, 2005, 127(41): 14348−14354.

[20] ZOU Jing-feng, MA Li-feng, JIA Wei-tao, LE Qi-chi, QIN Gao-wu, YUAN Yuan. Microstructural and mechanical response of ZK60 magnesium alloy subjected to radial forging [J]. Journal of Materials Science & Technology, 2021, 83: 228−238.

[21] WANG Hai-xuan, ZHANG Li-xin, CHEN Wen-zhen, FANG Da-qing, ZHANG Wen-cong, CUI Guo-rong. Improved tension/compression asymmetry achieved in high-strength magnesium alloys via compression-extrusion process [J]. Materials Science and Engineering: A, 2018, 736: 239−247.

[22] LIN Jin-bao, WANG Qu-dong, PENG Li-ming, ROVEN H J. Microstructure and high tensile ductility of ZK60 magnesium alloy processed by cyclic extrusion and compression [J]. Journal of Alloys and Compounds, 2009, 476(1/2): 441−445.

[23] LV Shu-hui, YANG Qiang, LV Xiao-ling, MENG Fan-zhi, QIU Xin. Effects of reduced extrusion temperature on microstructure and mechanical properties of Mg−6Zn−0.5Zr alloy [J]. Materials & Design, 2023, 225: 111568.

[24] SHE Jia, PENG Peng, TANG Ai-tao, ZHANG Jian-yue, MAO Jian-jun, LIU Ting-ting, ZHOU Shi-bo, WANG Yong-jian, PAN Fu-sheng. Novel on-line twist extrusion process for bulk magnesium alloys [J]. Materials & Design, 2019, 182: 108011.

[25] YUAN Yu-chun, MA Ai-bin, GOU Xiao-fan, JIANG Jing-hua, ARHIN G, SONG Dan, LIU Huan. Effect of heat treatment and deformation temperature on the mechanical properties of ECAP processed ZK60 magnesium alloy [J]. Materials Science and Engineering: A, 2016, 677: 125−132.

[26] WANG Wen-ke, CUI Guo-rong, ZHANG Wen-cong, CHEN Wen-zhen, WANG Er-de. Evolution of microstructure, texture and mechanical properties of ZK60 magnesium alloy in a single rolling pass [J]. Materials Science and Engineering: A, 2018, 724: 486−492.

[27] ZHANG Jian-yue, PENG Peng, LUO A A, SHE Jia, TANG Ai-tao, PAN Fu-sheng. Dynamic precipitation and enhanced mechanical properties of ZK60 magnesium alloy achieved by low temperature extrusion [J]. Materials Science and Engineering: A, 2022, 829: 142143.

[28] PAN Hu-cheng, QIN Gao-wu, HUANG Yun-miao, REN Yu-ping, SHA Xue-chao, HAN Xiao-dong, LIU Zhi-quan, LI Cai-fu, WU Xiao-lei, CHEN Hou-wen, HE Cong, CHAI Lin-jiang, WANG Yun-zhi, NIE Jian-feng. Development of low-alloyed and rare-earth-free magnesium alloys having ultra-high strength [J]. Acta Materialia, 2018, 149: 350−363.

[29] XU Jing, GUAN Bo, XIN Yun-chang, WEI Xue-dong, HUANG Guang-jie, LIU Cheng-lu, LIU Qing. A weak texture dependence of Hall−Petch relation in a rare-earth containing magnesium alloy [J]. Journal of Materials Science & Technology, 2022, 99: 251−259.

[30] YUAN W, PANIGRAHI S K, SU J Q, MISHRA R S. Influence of grain size and texture on Hall−Petch relationship for a magnesium alloy [J]. Scripta Materialia, 2011, 65(11): 994−997.

[31] LEE D H, LEE G M, PARK S H. Difference in extrusion temperature dependences of microstructure and mechanical properties between extruded AZ61 and AZ91 alloys [J]. Journal of Magnesium and Alloys, 2023, 11(5): 1683−1696.
[32] JIANG J, BRITTON T B, WILKINSON A J. Measurement of geometrically necessary dislocation density with high resolution electron backscatter diffraction: Effects of detector binning and step size [J]. Ultramicroscopy, 2013, 125: 1−9.
[33] WANG Hai-xuan, CHEN Wen-zhen, ZHANG Wen-cong, FANG Da-qing, WANG Song-hui, WANG Wen-ke. Improving the tension-compression asymmetry of ZK61 magnesium alloy through texture optimization in combined extrusion [J]. Materials Characterization, 2024, 207: 113599.
[34] KANG Jin-wen, WANG Cui-ju, DENG Kun-kun, NIE Kai-bo, BAI Yan, LI Wei-jian. Microstructure and mechanical properties of Mg−4Zn−0.5Ca alloy fabricated by the combination of forging, homogenization and extrusion process [J]. Journal of Alloys and Compounds, 2017, 720: 196−206.
[35] CHENG Wei-li, TIAN Quan-wei, YU Hui, ZHANG Hua, YOU B S. Strengthening mechanisms of indirect-extruded Mg−Sn based alloys at room temperature [J]. Journal of Magnesium and Alloys, 2014, 2(4): 299−304.
[36] TONDA H, ANDO S. Effect of temperature and shear direction on yield stress by $\{11\bar{2}2\}\langle\bar{1}\bar{1}23\rangle$ slip in HCP metals [J]. Metallurgical and Materials Transactions A, 2002, 33: 831−836.
[37] YANG Qiang, XIE Ze-feng, LI Jun, LV Shu-hui, ZHANG Wei, WU Rui-zhi, PAN Hu-cheng, LI Rong-guang, QIU Xin. ZK60 based alloys with high-strength and high-ductility: A review [J]. Resources Chemicals and Materials, 2023, 2(2): 151−166.
[38] SHI Feng-jian, PIAO Nan-ying, WANG Hao, WANG Ji-heng, ZANG Qian-hao, GUO Yu-hang, CHEN Cai, ZHANG Lu. Investigation of microstructure and mechanical properties of ZK60 magnesium alloy achieved by extrusion-shearing process [J]. Journal of Materials Research and Technology, 2023, 25: 799−811.
[39] ZHANG Jing, JOSHI S P. Phenomenological crystal plasticity modeling and detailed micromechanical investigations of pure magnesium [J]. Journal of the Mechanics and Physics of Solids, 2012, 60 (5): 945−972.
[40] CHRISTIAN J W, MAHAJAN S. Deformation twinning [J]. Progress in Materials Science, 1995, 39(1/2): 75−78.
[41] BARNETT M R, DAVIES C H J, MA X. An analytical constitutive law for twinning dominated flow in magnesium [J]. Scripta Materialia, 2005, 52(7): 627−632.
[42] BARNETT M R, KESHAVARZ Z, BEER A G, ATWELL D. Influence of grain size on the compressive deformation of wrought Mg−3Al−1Zn [J]. Acta Materialia, 2004, 52(17): 5093−5103.
[43] YIN S M, WANG C H, DIAO Y D, WU S D, LI S X. Influence of grain size and texture on the yield asymmetry of Mg−3Al−1Zn alloy [J]. Journal of Materials Science & Technology, 2011, 27(1): 29−34.
[44] MISHRA S, KHAN F, PANIGRAHI S K. A crystal plasticity based approach to establish role of grain size and crystallographic texture in the tension−compression yield asymmetry and strain hardening behavior of a magnesium−silver−rare earth alloy [J]. Journal of Magnesium and Alloys, 2022, 10(9): 2546−2562.

通过二次挤压快速凝固带材优化 ZK60 镁合金性能

李振帅[1,2]，杨 超[1,2]，包 帅[1,2]，陈云贵[1,3]

1. 四川大学 新能源与低碳技术研究院，成都 610207；
2. 四川大学 材料科学与工程学院，成都 610065；
3. 四川大学 后续能源材料与器件教育部工程研究中心，成都 610065

摘 要：采用光学显微镜、扫描电子显微镜、X 射线衍射、电子背散射衍射和力学测试等方法，研究了快速凝固(RS)和传统铸锭工艺生产的 ZK60 挤压合金的显微组织和力学性能。结果表明，RS ZK60 挤压合金具有较高的拉伸屈服强度(TYS)、压缩屈服强度(CYS)和伸长率，分别为 300.8 MPa、303.6 MPa 和 18.6 %。具有 1.28 μm 超细晶粒的 RS ZK60 挤压合金不仅具有最大极性密度为 3.3 的弱织构，而且 CYS/TYS 比值约为 1.0，解决了拉压不对称问题。强化机理计算表明，RS ZK60 挤压合金力学性能的改善主要源于晶粒细化。

关键词：ZK60 镁合金；快速凝固；热挤压；拉压不对称性；织构；强化机制

(Edited by Xiang-qun LI)